Acta Mechanica 148, 93–104 (2001)

ACTA MECHANICA

Viscoplastic response of a circular plate to an underwater explosion shock

Z. Zong and **K. Y. Lam,** Singapore, Singapore

(Received January 11, 2000; revised March 7, 2000)

Summary. Viscoplastic response of a fully-clamped circular plate to an underwater explosion shock is studied in this paper. Strain-rate effect is included in the response. A fluid-structure interaction model is introduced, which is characterized by two stages: In the early stage, only the shock wave in water is considered, and the motion of structure is neglected. In the second stage, the wave propagation in structure and fluid is disregarded, and only long-term fluid force (added mass) and long-term structural force (membrane stress) are considered. Based on this model, the equation of motion of a fully-clamped circular plate is established, the solutions of which are compared with two experiments. The calculated maximum plastic deformations from present model are close to the observed values. The dependence of maximum plastic deformation on charge weight, plate radius and material property is also discussed.

1 Introduction

There is large amount of experimental and theoretical work on the elastic responses of simple marine structures to an underwater explosion shock [1], [2], [3]. The cases of most interest, however, are those in which the structure under consideration is stressed beyond its elastic limit and permanent plastic deformation (explosion damage) results, which may become so large that the structure thins to the point of rupture. Explosion damage has been of a major concern in naval engineering since World War II [4]–[7]. Among various types of marine structures, circular plates are frequently used both in experiments and theoretical analysis [4], [5]. Several theories were also developed to predict dynamic plastic deformations of such plates [4], [8]. The deformations predicted from these theories were, however, about 30% to 70% lower than observed values.

In this paper, a new understanding of the nature of fluid-structure interaction is proposed to study the dynamic plastic deformation of a submerged fully-clamped circular plate under underwater shock loading. Based on this understanding, a fluid-structure interaction model is introduced, which is characterized by two stages: In the early stage, only the shock wave in water is considered, and the motion of structure is neglected as if the shock strikes a rigid plate. In the second stage, the wave propagation in structure and fluid is disregarded, and only long-term fluid force (added mass) and long-term structural stress (membrane stress) are considered. Strain-rate effects are considered using Cowper and Symonds constitutive equation [9]. Based on this model, the equation of motion of a fully-clamped circular plate is established, the solutions of which are compared with two experiments. The maximum deformations estimated from the present model are close to the observed values. Compared with other theories, the model in this paper is simple yet accurate enough. Further parametric studies show the dependence of maximum plastic deformation on charge weight, standoff distance and material properties.

2 Problem formulation

Consider a circular plate fully-clamped at its circumference as shown in Fig. 1. On one side of the plate is air, and on the other side is water. An underwater shock produced by an underwater explosion strikes on the plate, as a result of which the plate deforms so severe that permanent plastic deformation is developed. The standofff distance from the charge center to the plate center is R. An underwater shock is spherical, but in the vicinity of a plate far from the charge, it can be simplified as a plane shock wave as shown in Fig. 1 a. When the shock wave finally dies away, and the motion of plate ceases, maximum plastic deformation W_m is developed. It is our purpose in this paper to find the plastic deformation W_m produced by an underwater shock.

A shock load causes two distinct effects in a plate. The first is the so-called "early time response", and the other "long-term response" or "overall structural response". In early time response, the shock load causes elastic and plastic waves to propagate through the thickness of plate. The propagation of stress waves through the plate thickness can cause failure by spalling when the shock load is sufficiently severe. This phenomenon occurs in the same order of time that it takes a stress wave to propagate through the thickness of plate, and this type of

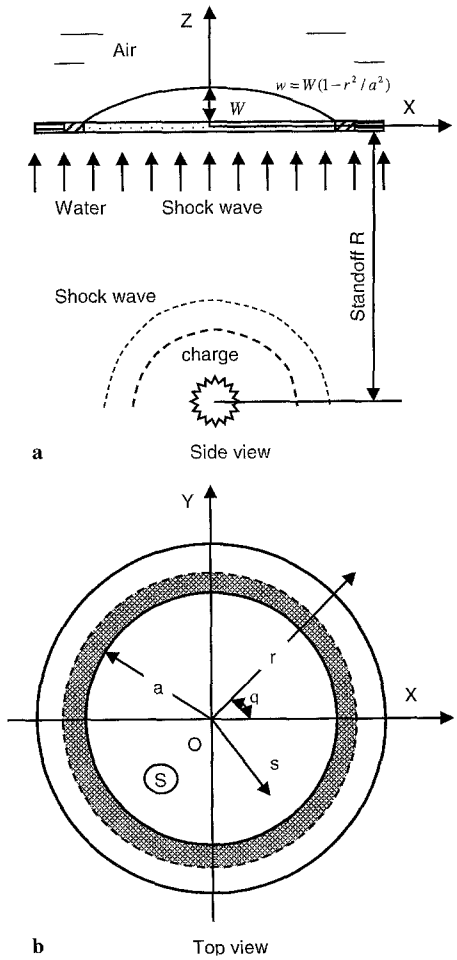

Fig. 1. Description of the problem

failure usually occurs within microseconds of initial shock striking. Following the early time response is overall structural response which occurs within millisecond of initial shock striking. Plastic deformation is of order of millisecond, and thus is overall structural response. The early time response is not considered in this paper. We focus on the long-term behavior of structures (typically of the order of milliseconds), for which the external shock dynamic load is assumed to impart momentum instantaneously to the middle surface of the plate (i.e., transverse wave propagation is disregarded) [10].

Corresponding to early time response is "early time loading" in water. In the linear approximation, there are totally three kinds of waves in water: One is incident wave produced by the release of high energy of an underwater explosion, one is reflected wave by the presence of the structure, and the last is radiating compressible wave developed by the structural motions. Corresponding to overall structural response is "inertial hydrodynamic force (added mass)" in water.

To account for long-term effects, the radiating compressible wave is negligible, but the inertial hydrodynamic force (added mass) induced by structure motions must be considered. Then, the fluid forces come from three sources: incident wave pressure in early time, reflected wave pressure in early time, and inertial hydrodynamic force (added mass). Based on such an understanding, we introduce the following fluid-structure interaction model, which is characterized by two stages: In the early stage, only the incident and reflected waves in water are considered, and the motion of structure is neglected as if the structure were absolutely rigid. In the second stage, the wave propagation in structure and fluid is disregarded, and only inertial hydrodynamic force and overall structural response are considered.

2.1 Plastic deformation

It is first assumed that a definite elastic limit σ_s exists, below which Hook's law applies and above which the plate acts like a membrane under a varying tension $\sigma_0(t)$. The nature of this plastic region depends on the material, but steel and copper can withstand very large strain (strain hardening) before finally rupturing. It is well established that, at the large strain rates of interest in explosion damage, σ_0 is much greater than for statically applied loads σ_s. There has been large amount of theoretical and experimental work on strain-rate effects, among which the following constitutive equation suggested by Cowper and Symonds [9] is widely accepted,

$$\dot{\varepsilon} = D\left(\frac{\sigma_0}{\sigma_s} - 1\right)^{1/q}, \qquad \sigma_0 \geq \sigma_s, \tag{1}$$

where ε is the dynamic strain, σ_0 is the dynamic flow stress at a uniaxial plastic strain rate $\dot{\varepsilon}$, D and q are constants for a particular material, and the overhead dot $[\dot{}\,] = d\cdot/dt$ is the derivative with respect to time. Equation (1) may be written as

$$\frac{\sigma_0}{\sigma_s} = 1 + \left(\frac{\dot{\varepsilon}}{D}\right)^{1/q}, \tag{2}$$

which, with $D = 40.4s^{-1}$ and $q = 5$, gives reasonable agreement with the experimental data for mild steel assembled by Symonds [11] as shown in Fig. 2. There is considerable scatter of the experimental data in Fig. 2. However, from an engineering viewpoint, Eq. (2) does provide a reasonable estimate of the strain rate sensitive uniaxial behavior of mild steel [10].

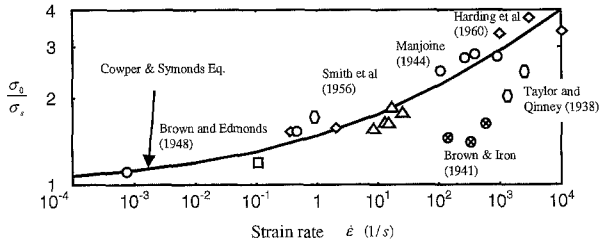

Fig. 2. Variation of dynamic uniaxial lower yield stress of mild steel with strain rate [11]

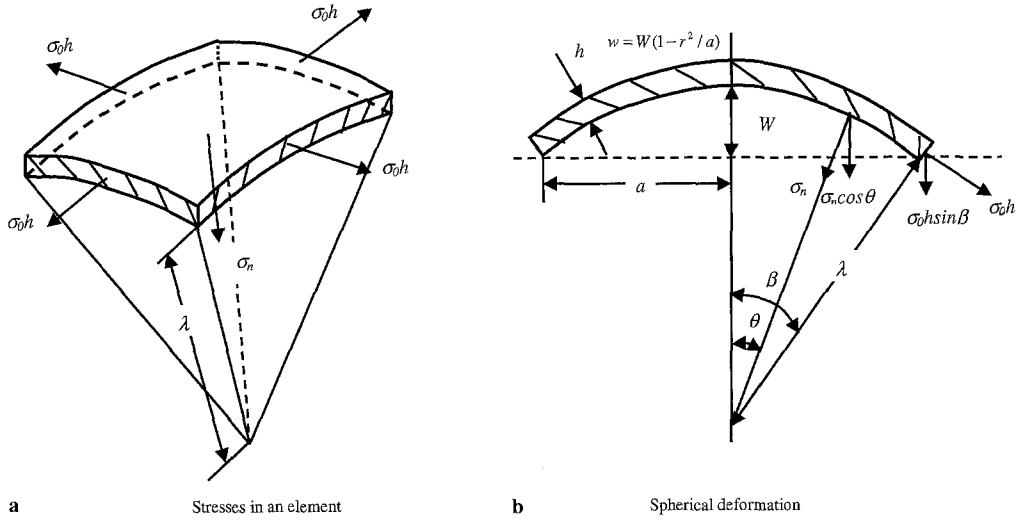

Fig. 3. Tangential and normal stress for a plate in plastic tension

There are two main stress components present in a plastically deformed plate: bending and membrane stresses. When the plastic deformation is large compared with plate thickness, bending stress is less significant than the membrane stress [12]. Thus, in our following analysis, only the membrane stress is considered. Then the plate yields once the stress σ_0 developed in the plate exceeds σ_s. The plastic deformation can also be described by a tangential stress equal to the tension σ_0, and the behavior of a plate becomes the same as that of a film under tension of magnitude $\sigma_0 h$ (see Fig. 3). Because the deformation profile of a membrane is spherical, we assume the deformation profile of the circular plate is given by

$$w(r,t) = W(t)\left(1 - \frac{r^2}{a^2}\right). \tag{3}$$

The surface area of such a plate is

$$A = \pi\left(a^2 + W^2\right) \tag{4}$$

from geometry. The area of the undeformed plate is $A_0 = \pi a^2$. Then the dynamic strain is given by

$$\varepsilon = \frac{(A - A_0)}{A_0} = \frac{W^2}{a^2}. \tag{5}$$

Substituting above equation in Eq. (2), we obtain the relation between strain rate and dynamic flow stress (tension)

$$\frac{\sigma_0}{\sigma_s} = 1 + \left[\frac{2W\dot{W}}{(a^2 D)}\right]^{1/q}, \tag{6}$$

Meanwhile, the plate thickness h also changes with time as $w(r,t)$ increases. Using Eq. (4) and applying the principle of mass conservation, we have

$$h\pi\,(a^2 + W^2)\,\varrho = h_0 \pi a^2 \varrho \tag{7}$$

where $h(t)$ is the plate thickness at time t, h_0 is the original plate thickness, and ϱ is the plate density. From above equation, we obtain the plate thickness at any time

$$h(t) = \frac{h_0 a^2}{a^2 + W^2} = \frac{h_0}{1+\varepsilon}\,. \tag{8}$$

The deformation of the plate into a curved profile described by Eq. (3) develops a normal stress component σ_n for unit area of the plate as shown in Fig. 3 a. The magnitude of σ_n can be calculated in the same way as for a film with surface tension. As shown in Fig. 3 b, the vertical component of the resultant tension along the circumference is

$$2\pi a \sigma_0 h \sin\beta = \frac{2\pi a^2 \sigma_0}{\lambda}\,, \tag{9}$$

where $\sin\beta$ is replaced by a/λ, and λ is the radius of curvature. The vertical component of the resultant normal stress is

$$\int_0^{\beta} (2\pi\lambda^2 \sin\theta)\,(\sigma_n \cos\theta)\,d\theta = \pi\lambda^2 \sigma_n \sin^2\beta = \pi a^2 \sigma_n\,, \tag{10}$$

where θ is the angle formed between vertical axis and radial direction. Because we assume in Eq. (3) that the deformation profile is spherical, the radius of curvature λ is independent of the angle θ. The vertical component of the resultant normal stress must be equal to that of the resultant tension along the circumference, that is

$$\frac{2\pi a^2 \sigma_0 h}{\lambda} = \pi a^2 \sigma_n\,,$$

from which we find normal stress σ_n to be of the form:

$$\sigma_n = \frac{2\sigma_0 h}{\lambda}\,. \tag{11}$$

From Fig. 3 b, we have

$$\sqrt{\lambda^2 - a^2} = \lambda - W\,,$$

from which, we further obtain

$$\lambda = \frac{a^2 - W^2}{2W}\,. \tag{12}$$

Substituting Eq. (12) in Eq. (11), we obtain:

$$\sigma_n = \frac{4\sigma_0 hW}{a^2 - W^2} \,. \tag{13}$$

This is the normal stress developed in the plate. σ_0 is given by Eq. (6), and h is given by Eq. (8).

2.2 Fluid forces

The basic assumption is that the motion of plate is negligible shortly after the arrival of the shock wave as if the shock wave struck an absolutely rigid undeformable plate. In the linear approximation, if the incident wave pressure is $P_I(r,t)$ and the reflected wave pressure is $P_S(r,t)$, the resultant pressure on the plate is $P_D = P_I + P_S$. The diffraction effect is negligible in the early stage, and we have $P_S = P_I$. So, the resultant pressure is

$$P_D = 2P_I \,, \tag{14}$$

This equation is valid if $P_I \leq 1.2 \times 10^8$ N/m^2, above which nonlinear effect should be considered.

Underwater explosion shock waves are characterized by a sharp rise in pressure followed by a quick decay in time. The pressure-time curve can be approximated by an exponential function of the form:

$$P_I = P_m \exp\left(\frac{-t}{\tau}\right). \tag{15}$$

The similarity solutions for peak pressure P_m and time decay constant τ are

$$P_m = 2.786 \times 10^7 \left(\frac{G^{1/3}}{R}\right)^{1.18} \text{N/m}^2 \,, \qquad \tau = 0.581\,8\, G^{1/3} \left(\frac{G^{1/3}}{R}\right)^{-0.185} \text{ms} \,, \tag{16}$$

where G is charge weight in kg, R is standoff distance in meter [6].

After the shock wave strikes the plate, the plate sets into motion with velocity described by

$$\frac{dw}{dt} = \frac{dW}{dt}\left(1 - \frac{r^2}{a^2}\right). \tag{17}$$

Such velocity produces a disturbance in water, the motion of which is assumed irrotational and incompressible. Then there exists a potential φ satisfying

$$\begin{aligned} \nabla^2\varphi &= 0 \,, && \text{throughout fluid domain} \\ \mathbf{n}\cdot\nabla\varphi &= \frac{\partial\varphi}{\partial n} = \frac{dw}{dt} \,, && \text{on the plate,} \\ |\nabla\varphi| &\to 0 \,, && \text{at infinity,} \end{aligned} \tag{18}$$

where $\mathbf{n}$ is the normal vector of the plate. Application of Green's theorem gives the solution to the above equation on the plate in the form of (see Fig. 1 b)

$$\varphi(\mathbf{r},t) = \frac{1}{2\pi}\iint\limits_S \frac{\partial\varphi}{\partial n}\frac{1}{|\mathbf{r}-\mathbf{s}|}\,dS = \frac{1}{2\pi}\iint\limits_S \frac{dW}{dt}\left(1 - \frac{s^2}{a^2}\right)\frac{1}{|\mathbf{r}-\mathbf{s}|}\,dS \,, \tag{19}$$

where ϱ_0 is water density. Then, the pressure on the plate is given by the linearized Bernoulli's equation.

$$P_R(\mathbf{r},t) = -\varrho_0 \frac{\partial \varphi}{\partial t} = -\frac{\varrho_0}{2\pi} \iint \frac{d^2W}{dt^2} \left(1 - \frac{s^2}{a^2}\right) \frac{1}{|\mathbf{r}-\mathbf{s}|}\, dS\,. \tag{20}$$

The pressure at the center of the plate is then

$$\begin{aligned} P_R(0,t) &= -\frac{\varrho_0}{2\pi} \iint \frac{d^2W}{dt^2} \left(1 - \frac{s^2}{a^2}\right) \frac{1}{|\mathbf{s}|}\, dS \\ &= -\frac{\varrho_0}{2\pi} \int_0^{2\pi} dq \int_0^a \frac{d^2W}{dt^2} \left(1 - \frac{s^2}{a^2}\right) ds = -\frac{2\varrho_0 a}{3} \frac{d^2W}{dt^2}\,. \end{aligned} \tag{21}$$

Combining Eqs. (14) and (21), we obtain the resultant pressure at the center of the plate

$$P(0,t) = P(t) = P_D + P_R = 2P_I(t) - \frac{2\varrho_0 a}{3} \frac{d^2W}{dt^2}\,. \tag{22}$$

The first term is early time loading. The second term, of same order of plate acceleration, is inertial hydrodynamic force (added mass), which is a long-term loading.

2.3 The motion of plate under plastic tension

Hopkins and Prager [13] have shown that a fully-clamped circular plate yields once $P_D = 2P_I > P_c$, where P_c is the collapse pressure of a uniformly loaded circular plate. P_c is given by

$$P_c = 11.26 \frac{\sigma_s {h_0}^2}{4a^2} = 2.815 \frac{\sigma_s {h_0}^2}{a^2}\ (\mathrm{N/m^2})\,. \tag{23}$$

If a deforming plate is assumed to have geometrically similar profiles at all times, only the equation of motion for an element of the plate need be solved, as this solution determines the rest of the profile. For example, consider the assumed parabolic deformation of a circular plate given by Eq. (3) subject to a pressure $P(t)$ at its center and a stress normal to the surface as a result of its deformation. If m is the mass of unit area of the plate, the equation of motion for unit area at the center of the plate is

$$m\frac{d^2W}{dt^2} = P(t) - \sigma_n(t)\,. \tag{24}$$

Substituting Eqs. (13), (22) in Eq. (24), we obtain the equation of motion:

$$m\,\frac{d^2W}{dt^2} = 2P_I(t) - \frac{2\varrho_0 a}{3}\,\frac{d^2W}{dt^2} - \frac{4\sigma_0 hW}{a^2 - W^2}\,. \tag{25}$$

which, after re-arranged, becomes

$$\left(m + \frac{2\varrho_0 a}{3}\right) \frac{d^2W}{dt^2} + \frac{4\sigma_0 hW}{a^2 - W^2} = 2P_m \exp\left(\frac{-t}{\tau}\right). \tag{26}$$

This equation can only be numerically solved together with Eqs. (6) and (8). Writing in the form of the system of equations, we have:

$$\begin{aligned}
\frac{dW}{dt} &= V, \\
\frac{dV}{dt} &= \left[2P_m \exp\left(\frac{-t}{\tau}\right) - \frac{4\sigma_0 hW}{a^2 - W^2}\right]\left(m + \frac{2\varrho_0 a}{3}\right), \\
\sigma_0 &= \sigma_s\left[1 + \left(\frac{2WV}{a^2 D}\right)^{1/q}\right], \\
h &= \frac{h_0 a^2}{a^2 + W^2}\,.
\end{aligned} \tag{27}$$

The above equations can be easily solved using ordinary Runge-Kutta method.

3 Comparison and discussions

Two experiments are used in this section to check the validity of the equations derived in the foregoing sections. The first experiment was made by Goranson [4]. The plate used in the experiment was made of steel. The explosive was TNT, the pressures produced by which on the plate is given in Table 1, denoted as Steel 1. The material properties and geometry of the plate are given in Table 2. The steel plate, which were 0.532 8 meters in diameter and 2.79 mm thick, were deformed by 0.453 6 kg TNT charges. The central deformations was 0.03 meters at standoff distance 1.827 meters. The time t_m to the maximum deformation was not given. Based on early time loading model, Goranson calculated the central deformations, which is given in Table 3. The calculated value is only half the observed value. Because Goranson used energy method, his model could not estimate t_m. Goranson's theory was later improved by Kirkwood and Richardson [8]. The result predicted by this improved theory is also given in Table 3. Although it is improved over Goranson's result, Kirkwood's result is still 33% lower than the observed value.

Table 1. Explosive (TNT) and pressures on the plates

	Steel 1	Steel 2
Charge weight W (kg)	0.45	7.65
Standoff distance R (m)	1.827	2.132
Peak pressure P_m (N/m^2)	$1.873\,25 \times 10^7$	$4.759\,64 \times 10^7$
Time decay τ (s)	$0.807\,953 \times 10^{-4}$	$1.794\,91 \times 10^{-4}$

Table 2. Material properties and geometry of the plates

	Steel 1	Steel 2
Radius a (m)	0.266 4	0.043 14
Thickness h (m)	0.002 79	0.002 03
Yield stress σ_s (N/m^2)	2.4×10^8	2.4×10^8
Density ϱ (kg/m^3)	7 800	7 800
Collapse pressure P_c (N/m^2)	$0.926\,3 \times 10^5$	1.469×10^6

Table 3. Comparison of theoretical and experimental results

		Steel 1	Steel 2
W_m	Goranson [4]	0.015	0.008 2
(m)	Kirkwood [8]	0.020	0.018 7
	Present paper	0.028	0.027
	Experimental	0.03	0.024
t_m	Goranson [4]	Not available	Not available
(ms)	Present paper	2.8	0.27
	Experimental	Not available	Not available

Using Eq. (27), we calculated the central deformation of the steel plate, with result given in Table 3. The calculated and observed values are very close. The time history of central deformation and time history of central velocity are shown in Fig. 4.

Figure 5 shows the history of dynamic stress flow. The dynamic stress flow σ_0 rises from $\sigma_s = 240$ MN/m^2 to 400 MN/s^2 in 1.5 ms, after which the dynamic stress flow does not change with time further.

In the second experiment [4], the circular plate is made of steel, too. The properties and geometry of the plate are given in Table 2, denoted as Steel 2. The charge is 4.5 kg TNT. The maximum deformation from the experiment is given in Table 3. The central deformation and the time t_m calculated from Eq. (27) are given in the same Table. The maximum deformations estimated from Eq. (27) and obtained from the experiment are in good agreement. The maximum plastic deformations calculated from Goranson's theory and Kirkwood's improved theory are both lower than the experimental value.

The above experiments validated the model introduced in this paper. Although we used simple assumptions, the results turned out to be better than other thories. The main difference between the present model and former theories is that long-term effects both present in fluid and plate are considered in this paper.

Figure 6 shows the effects of strain rate and long-term fluid force (added mass) based on Eq. (27). Four cases are considered. The solid lines are the time histories of maximum plastic deformations calculated from Eq. (27) with both strain rate effect and added mass effect considered. The dotted lines show the case that only added mass effect is considered with strain rate effect disregarded. The dashed lines show the strain rate effect with added mass effect neglected. The dashed-dotted lines show the case with both strain rate effect and added mass effect neglected.

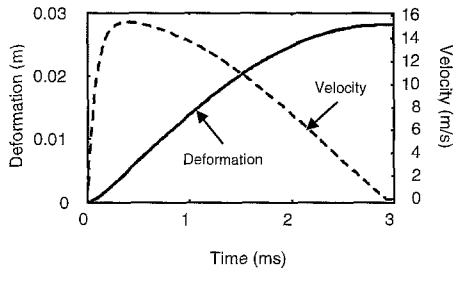

Fig. 4. Time history of central deformation and time history of central velocity

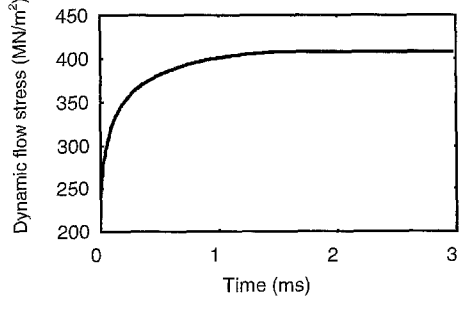

Fig. 5. Time history of dynamic flow stress

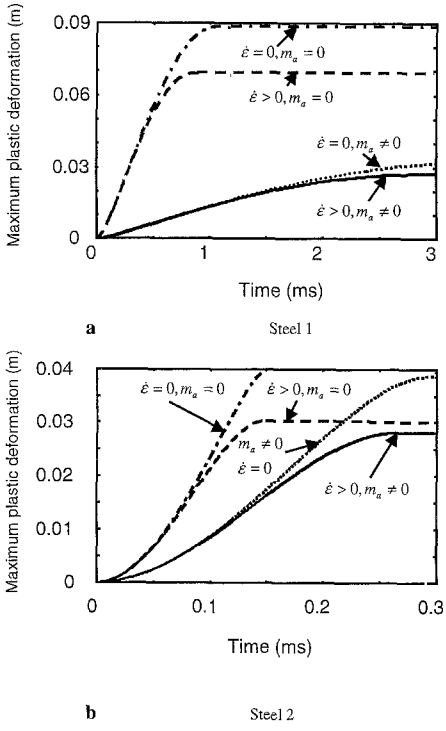

Fig. 6. The effects of strain rate and added mass on maximum plastic deformation. $\varepsilon > 0$ means the strain rate effect is considered. $\dot{\varepsilon} = 0$ means the strain rate effect is not considered. $m_a \neq 0$ means added mass is considered while $m_a = 0$ means added mass is not considered

For Steel 1 as shown in Fig. 6 a, strain rate effect is small while added mass effect is significant. The final maximum plastic deformation with added mass considered is less than half that with added mass not considered (compare the dashed line and solid line in Fig. 6 a). The strain rate effect is, however, much small as the dotted and solid lines show in the figure.

For Steel 2 as shown in Fig. 6 b, strain rate effect is more significant than added mass effect. The final maximum plastic deformation with strain rate effect considered is about 30% lower than that with strain rate effect neglected (see the dotted and solid lines in Fig. 6 b). On the other hand, the two results with added mass considered or not are slightly different. Nevertheless, Fig. 6 shows that both strain rate and added mass have important effects. Their effects are case-dependent.

To investigate the dependence of maximum plastic deformation on other factors, three charge weights (W = 1 kg, 10 kg, 20 kg), and three plate radii (a = 0.5 m, 0.75 m, 1.0 m) are used in our calculations. The plate thickness is assumed to be 0.005 m. Figure 7 shows the relation between standoff distance and maximum deformation for steel, which properties are given in Table 2. Figure 8 shows the relation between standoff distance and the time t_m to the maximum deformation.

Figure 7 shows that maximum deformation is a decreasing function of standoff distance, which results from the decreasing dependence of peak pressure on standoff distance, see Eq. (16). Moreover, the larger the radius is, the smaller the maximum plastic deformation is. This can be seen from Fig. 7 a through Fig. 7 c. The physical reason is that large radius induces more fluid into motion, which absorbs more kinetic energy, and thus less energy is imparted into the plate.

Figure 8 shows the dependence of the time t_m on standoff distance. It can be seen that t_m is weakly dependent on standoff distance. On the contrary, comparison of Fig. 8 a through Fig. 8 c shows that t_m is strongly dependent on the plate radius. When the radius increases

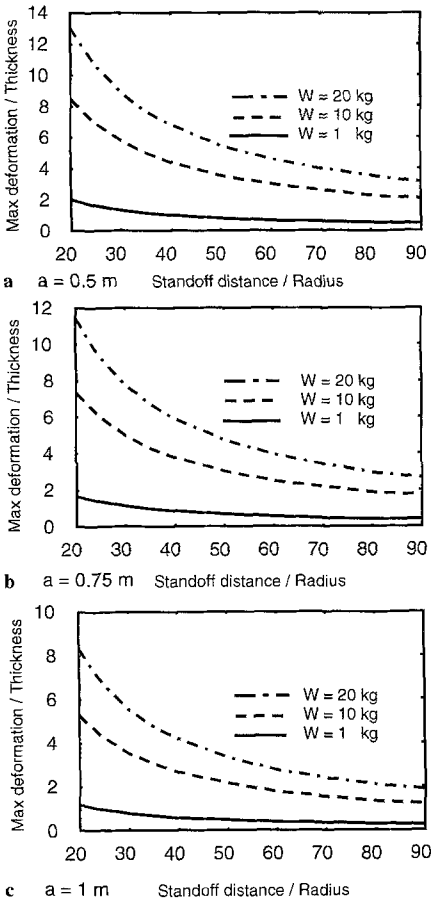

Fig. 7. Relationship between standoff distance and maximum plastic deformation for Steel (thickness = 0.005 m)

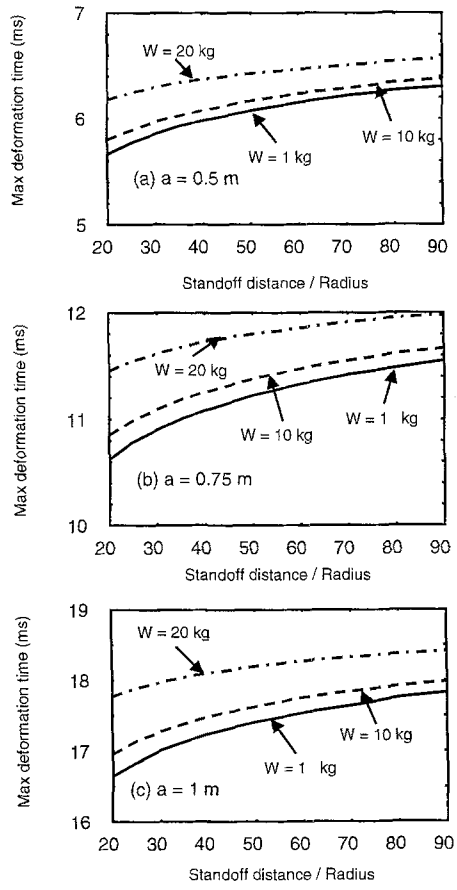

Fig. 8. Relationship between standoff distance and maximum deformation time for Steel (thickness = 0.005 m)

from 0.5 m to 1 m, t_m increases from about 6 ms to 17 ms. So, it takes more time for a bigger plate to reach final plastic deformation than a smaller plate. This is in accord with our intuition.

4 Conclusions

In this paper a fluid-structure model was introduced, which is characterized by two stages: In the early stage, only the shock wave in water is considered, and the motion of the structure under consideration is neglected. In the second stage, the wave propagation in structure and fluid is disregarded, and only the long-term forces (added mass and membrane force) are considered. Based on this model, the equation of motion of a fully-clamped circular plate is established, the solutions of which were compared with two experiments. The calculated values are very close to the observed values, validating the model proposed in this paper.

In the above model, strain rate effect is also included. It is shown in the paper that both strain rate and added mass have significant effects on the maximum plastic deformations. But, their effects are case-dependent.

The dependence of plastic deformations on standoff distance, charge weight and radius is also discussed.

References

[1] Huang, H.: Transient interaction of plane acoustic waves with a spherical elastic shell. J. Acoust. Soc. Am. **45,** 661 – 770 (1969).
[2] Huang, H.: An exact analysis of the transient interaction of acoustic plane waves with a cylindrical elastic shell. J. Appl. Mech. **37,** 1091 – 1100 (1970).
[3] Huang, H., Wang, Y. F.: Transient interaction of spherical acoustic waves with a cylindrical elastic shell. J. Acoust. Soc. Am. **48,** 228 – 235 (1970).
[4] Cole, R. H.: Underwater explosion. Princeton: Princeton University Press 1948, pp. 353 – 424.
[5] Jones, R. A., Shin, Y. S.: Experimental investigation of the response and failure mechanisms of circular metal and composite plates to underwater explosion. In: 61st Shock and Vibration Symposium, Pasadena, Ca. 1990, pp. 163 – 178.
[6] Zong, Z., Lam, K. Y., Liu, G. R.: Propabilistic risk prediction of submarine pipelines subjected to underwater shock. ASME J. Offshore Mech. Arctic Eng. **121,** 251 – 254 (1999).
[7] Zong, Z., Lam, K. Y., Liu, G. R.: Numerical investigations of damaging effects of underwater shock on submarine structures in the presence of free surface. In: 69th Shock and Vibration Symposium, St. Paul, MN. 1998, pp. 10: 1 – 8.
[8] Kirkwood, J. G., Richardson, J. M.: The plastic deformation of circular diaphragms under dynamic loading by an underwater explosion wave. OSRD 4200 (1944).
[9] Cowper, G. R., Symonds, P. S.: Strain hardening and strain-rate effects in the impact loading of cantilever beams. Brown University Division of Applied Mathematics Report No. 28 (1957).
[10] Jones, N.: Structural Impact, Cambridge: Cambridge University Press 1989, pp. 333 – 383.
[11] Symonds, P. S.: Survey of methods of analysis for plastic deformation of structures under dynamic loading. Brown University, Division of Engineering Report, BU/NSRDC/1-67 (1967).
[12] Jones, N.: A Theoretical study of the dynamic plastic behavior of beams and plates with finite-deflections. Int. J. Solids Struct. **7,** 1007 – 1029 (1971).
[13] Hopkins, H. G., Prager, W.: The load carrying capacities of circular plates. J. Mech. Phys. Solids **2,** 1 – 13 (1953).

Authors' address: Z. Zong and K. Y. Lam, Institute of High Performance Computing, 89C Science Park Drive, #02-11/12, The Rutherford, Singapore Science Park I, Singapore 118261